Early Warning of Abnormal Train-Induced Vibrations for a Steel-Truss Arch Railway Bridge: Case Study

You-Liang Ding, Ph.D.[1]; Han-Wei Zhao, S.M.ASCE[2]; Lu Deng, Ph.D., M.ASCE[3]; Ai-Qun Li, Ph.D.[4]; and Man-Ya Wang[5]

Abstract: Considering the new challenges for high-speed railway bridges, the early warning of abnormal train-induced vibrations is necessary for ensuring the operation safety of both the bridge structures and the trains on the bridge. In this study, an online monitoring system for detecting abnormal train-induced vibration responses is developed, and the Dashengguan Yangtze River Bridge is used for illustration. First, to accurately investigate the influence of different train lanes and the number of carriages on train-induced vibrations, the speed-acceleration (train speed-bridge acceleration) correlations under different loading cases are obtained using an online identification method. Then, a two-stage method for early warning of abnormal train-induced acceleration responses of the bridges is developed using wavelet packet decomposition and interval estimation theory. Finally, the early warning method for identifying abnormal train-induced transverse vibrations is presented. The results show that (1) the train lane and the number of carriages affect the speed-acceleration correlations, and the identification of loading cases is needed for the accurate monitoring of speed-acceleration correlations; (2) by using wavelet packet decomposition, the median line of speed-acceleration correlations can be optimally extracted, and the early warning thresholds for abnormal train-induced acceleration responses can be properly determined using the interval estimation theory compared with the point estimation theory; and (3) the train running parameters of the Dashengguan Yangtze River Bridge are all within safe limits, but the wheel unloading rate and derailment coefficient have reached 60% of the limits due to the train-induced transverse vibrations. The effects of train-induced transverse vibration on the train running stability is worthy of attention. **DOI: 10.1061/(ASCE)BE.1943-5592.0001143.**

Author keywords: Structural health monitoring; Steel-truss arch railway bridge; Train-induced vibration; Early warning threshold; Train running parameter.

Introduction

High-speed railways have provided remarkable convenience for passenger transportation, and bridges play a vital role. Because high-speed trains are one of the main excitation sources for high-speed railway bridges in service, the bridge vibration responses under the excitation of trains become an important research topic in bridge engineering.

The numerical simulation for dynamic responses of bridges under the action of high-speed trains is an important research focus in bridge engineering. Ju and Lin (2003a), Lacarbonara and Colone (2007), and Zhao et al. (2017) studied the dynamic responses of arch bridges induced by high-speed trains. Dinh et al. (2009) explored the bridge dynamic responses using a three-dimensional bridge-train interaction model considering the wheel–rail contact. Zou et al. (2016) predicted the upper and lower bounds of vehicle-induced bridge responses using the interval analysis method. The high running speed is an important characteristic for high-speed railway bridges, and a higher train speed generally results in more significant dynamic responses. Many studies have focused on the train speeds at which the resonance of the train-bridge system may occur. Li and Su (1999) established the formula of bridge response for a simply supported girder bridge under the action of high-speed trains and analyzed the train speeds that lead to the train-bridge resonance. Ju and Lin (2003b), Martinez-Rodrigo et al. (2010), and Xia et al. (2006) investigated the vibration mechanism of existing high-speed railway bridges under train loads and discussed the critical speed of resonance. Mao and Lu (2013) analyzed the critical speed that leads to resonance and put forward a Z-factor to describe the severity of bridge resonance. Deng et al. (2015) analyzed the speed influence on the dynamic impact factors for shear and bending moment of both simply supported and continuous concrete girder bridges using a vehicle-bridge vibration model. However, numerical simulation cannot fully consider all the factors that affect the vibration of the train-bridge system, such as the environmental effects, track irregularities, and other random factors.

With the rapid development of testing technologies in civil engineering, the vibration responses of railway bridges under the action of high-speed trains can be accurately measured. Some promising work considering vehicle-induced bridge vibrations, which is based on field tests or structural health monitoring (SHM) systems, has been conducted in recent years. Ju et al. (2009) studied the dominant

[1]Professor, Key Laboratory of C&PC Structures of the Ministry of Education, Southeast Univ., Nanjing 210096, China (corresponding author). ORCID: https://orcid.org/0000-0002-0774-426X. E-mail: civilchina@hotmail.com

[2]Ph.D. Student, School of Civil Engineering Key Laboratory of C&PC Structures of the Ministry of Education, Southeast Univ., Nanjing 210096, China. E-mail: wudizhw_0@126.com

[3]Professor, College of Civil Engineering, Hunan Univ., Changsha, Hunan 410082, China. E-mail: denglu@hnu.edu.cn

[4]Professor, Beijing Advanced Innovation Center for Future Urban Design, Beijing Univ. of Civil Engineering and Architecture, Beijing 100044, China; School of Civil Engineering, Southeast Univ., Nanjing 210096, China. E-mail: liaiqun@bucea.edu.cn

[5]Ph.D. Student, School of Civil Engineering Key Laboratory of C&PC Structures of the Ministry of Education, Southeast Univ., Nanjing 210096, China. E-mail: civilmail16@163.com

Note. This manuscript was submitted on December 19, 2016; approved on May 31, 2017; published online on September 8, 2017. Discussion period open until February 8, 2018; separate discussions must be submitted for individual papers. This paper is part of the ***Journal of Bridge Engineering***, © ASCE, ISSN 1084-0702.

frequencies of train-induced bridge vibrations based on the measured accelerations. Xia and Zhang (2005), He et al. (2008), Mellat et al. (2014), and Feng and Feng (2015) used field test results or the SHM system to update the finite-element (FE) model and analyzed the dynamic response of railway bridges. Nonetheless, most of these studies were based on the analysis of short-term data, which cannot reflect the long-term degradation of railway bridges.

The effects of high-speed trains (e.g., fatigue) and the environment (e.g., corrosion) will continuously deteriorate the performance of high-speed railway bridges and the train running stability. Although it may not result in catastrophic failure of bridge structures, it causes changes in bridge vibration performance, leading to passenger discomfort or premature wearing of rail vehicle wheels. Therefore, early detection of abnormal train-induced vibration responses based on long-term monitoring data is of great interest to bridge management. In view of this challenge, this paper presents a case study of two early warning methods for abnormal train-induced vibration responses of the Dashengguan Yangtze River Bridge. The first method is based on the acceleration responses of the bridge, which aims to ensure the serviceability of the bridge regarding passenger discomfort. The second method is based on the transverse vibrations of the bridge, which aims to ensure running stability of high-speed trains and to prevent derailment. The detailed process of the two early warning methods is introduced using the long-term monitoring data from January 1, 2014 to December 31, 2015, and the warning thresholds are determined for the Dashengguan Yangtze River Bridge based on analysis of the monitoring data.

Case Study

Bridge Description and Monitoring System

The Dashengguan Yangtze River Bridge is the longest six-lane high-speed railway bridge in the world. It has two 336-m long main spans and consists of six lanes, including two lanes on the downstream side for the Beijing-Shanghai (B-S) high-speed railway, two lanes on the upstream side for the Shanghai-Wuhan-Chengdu (S-W-C) Railway, and two lanes on the outer sides of the bridge deck for the Nanjing Metro. The four lanes of the B-S high-speed and S-W-C railways have been put into operation. The design load of the six lanes is more than 600 kN/m along the longitudinal direction of the bridge. The design train speed of 300 km/h is among the highest in the world. As shown in Fig. 1, the bridge consists of two continuous steel-truss arches and approach spans, with a span configuration of $108 + 192 + 2 \times 336 + 192 + 108$ m. As shown in Fig. 2, the arches feature three main trusses spaced 15 m apart in the transverse direction.

Because of the unusual characteristics of the Dashengguan Yangtze River Bridge, including the long span of the main girders, the heavy design loads, and the high train speeds, a long-term SHM system was installed. In this monitoring system, acceleration sensors are used to measure the dynamic responses of the bridge. The bridge sections on which acceleration responses are measured are shown in Fig. 1. Six sections are instrumented, among which Section 1 is on the end span on the Beijing side, Section 2 is on the side span on the Beijing side, Section 3 is on the middle span on the Beijing side, Section 4 is on the middle span on the Shanghai side, Section 5 is on the side span on the Shanghai side, and Section 6 is on the end span on the Shanghai side. A vertical acceleration sensor is used at Sections 1 and 6. A vertical acceleration sensor and a transverse are used at Sections 2–5. The locations of acceleration sensors in their measured sections are show in Fig. 2. The sampling rate of the acceleration sensors is set to 200 Hz. All acceleration data measured in the Dashengguan Yangtze River Bridge are filtered with a low-pass digital filter of 20 Hz to reduce the high-frequency noise in the dynamic signals, and the acceleration responses of the bridge under the action of high-speed trains are finally obtained. In addition, the SHM system on the Dashengguan Yangtze River Bridge also includes fiber Bragg grating (FBG) strain sensors (Fig. 2), FBG thermal sensors, and speedometers to monitor the strain of key structural members, the temperature of the bridge structure, and the train speeds, respectively.

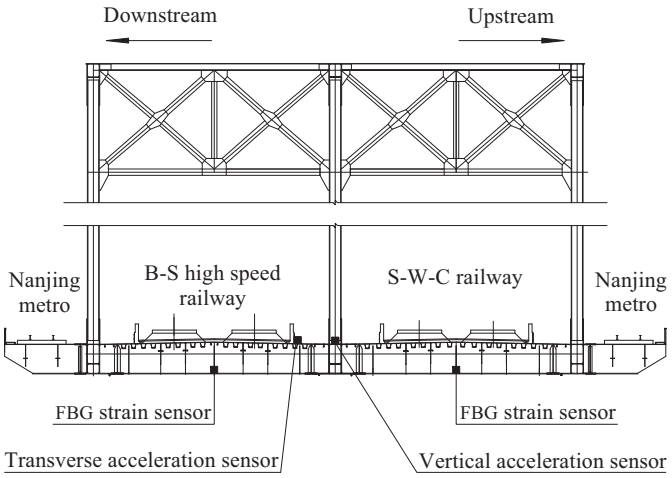

Fig. 2. Locations of the acceleration sensors (Note: FBG = fiber Bragg grating)

Bridge Acceleration Responses under the Action of High-Speed Trains

To investigate the long-term vibration performance of the Dashengguan Yangtze River Bridge under the action of high-speed trains, the maximum amplitudes (absolute values) of bridge acceleration in each measured section when each train crosses the bridge were calculated.

When a train crosses the bridge, the speedometer will record its train speed and crossing time, and the corresponding maximum amplitude of the train-induced acceleration responses can be obtained from the acceleration sensor. The train load is the main excitation of the high-speed railway bridges. Therefore, it is important to

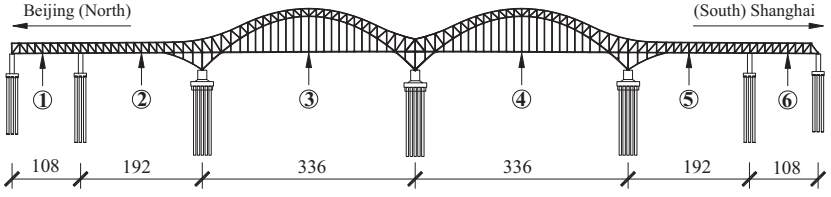

Fig. 1. Dashengguan Yangtze River Bridge and acceleration measurement sections (Units: meters)

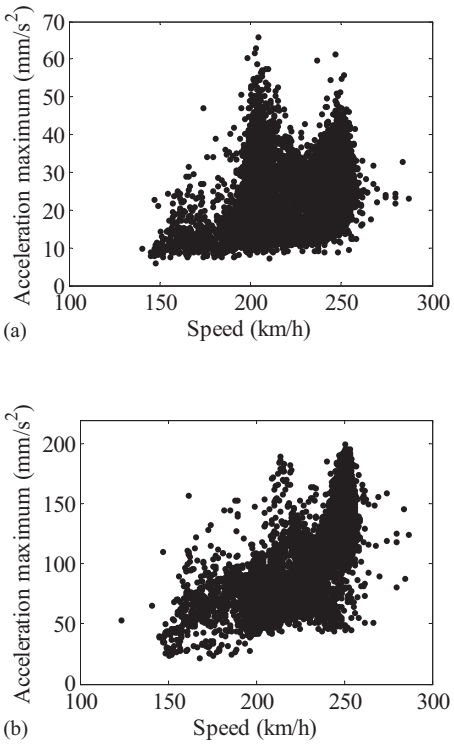

Fig. 3. Scatterplots of bridge acceleration and train speed: (a) transverse vibration; (b) vertical vibration

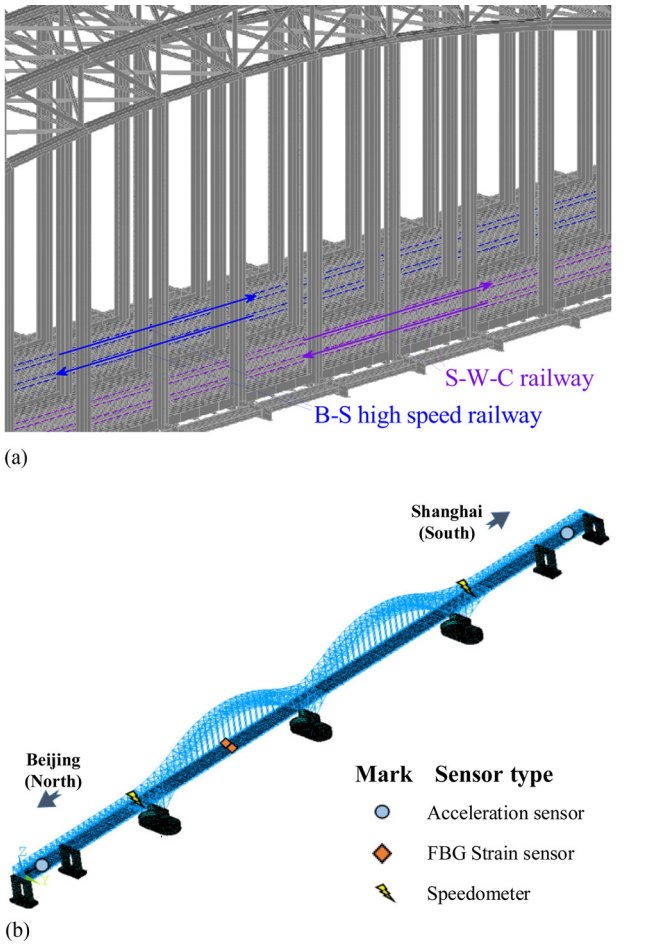

Fig. 4. Online identification of loading cases: (a) railway lanes of the Dashengguan Yangtze River Bridge; (b) selected sensors for online identification of loading cases

understand the influence of train speed on the acceleration response of the bridge. The relationship between the collected bridge accelerations and the train speed data is described using scatterplots. Fig. 3 shows the scatterplots of acceleration amplitudes in Section 2 in both the transverse and vertical directions and train speed from January 1, 2014 to December 31, 2015. As seen in Fig. 3, the data of the bridge acceleration and train speed show no obvious correlation. This is because the four running lanes of the Dashengguan Yangtze River Bridge and different types of high-speed trains (with 8 or 16 carriages) generate different speed-acceleration correlations. Therefore, the correlation scatterplots of speed acceleration without considering different loading cases cannot accurately reflect the train-induced vibration of the bridge. It is necessary to analyze the correlation scatterplots of speed acceleration in different loading cases to investigate the train-bridge interaction accurately.

Methodology

Correlation Analysis of Speed Acceleration Based on Online Identification of Loading Cases

The Dashengguan Yangtze River Bridge carries four high-speed railway lanes: two lanes of the B-S high-speed railway (250 km/h or higher speeds) and two lanes of the S-W-C railway (200 km/h or higher speeds), respectively [Fig. 4(a)]. The bridge acceleration responses are influenced by the different railway lines (B-S high-speed railway or S-W-C railway), the location of the train lane (loads in different lanes create eccentric loads of different magnitudes), and the number of carriages of a train. The speedometer installed on the bridge can only obtain the train speed data. The information of running lines, running direction (running lane), and number of carriages of the crossing train cannot be directly obtained from the speedometer. To analyze the correlation between the bridge acceleration response and the train speed in different loading cases, an online identification of loading cases for bridge vibration responses was developed. The SHM system installed on the Dashengguan Yangtze River Bridge includes various sensors (acceleration sensors, FBG strain sensors, and speedometers), and the online identification of loading cases can be conducted by the proper selection of sensor signals from the acceleration and FBG strain sensors [Fig. 4(b)] as shown in the following:

1. Identification of different railway lines: As shown in Fig. 5(a), the occurrence of obvious peaks from the signal of FBG strain sensors installed on the diaphragms of two box girders (Fig. 2) are used to determine the railway line.
2. Identification of different running directions: From the time the speedometer begins to record the train speed, the data of the acceleration sensors installed at the two ends of the bridge are used to determine the running direction of the train. As shown in Fig. 5(b), the two signals are collected from the two acceleration sensors in Section 1 (Beijing side) and Section 6 (Shanghai side) of the bridge when a train crosses the bridge from Beijing (North) to Shanghai (South). The solid line is the signal from Section 1, and the dashed line is the signal from Section 6. It can be seen that the vibration of Section 1 occurs earlier than Section 6, indicating that the Beijing side is first subjected to the train loading, which reflects the fact that the train runs from Beijing (North) to Shanghai (South).

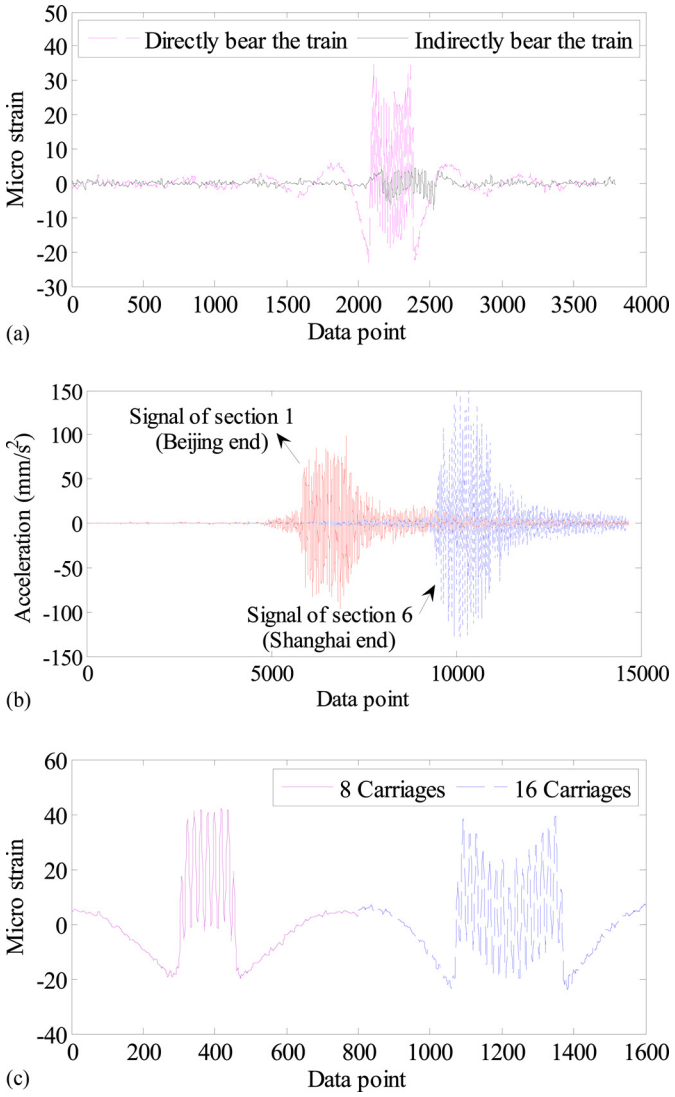

Fig. 5. Online identification for loading cases: (a) different railway lines (data of the FBG strain sensor under B-S high-speed railway); (b) different running direction (data of the acceleration sensors in Sections 1 and 6); (c) different numbers of carriages (data of the FBG strain sensor under B-S high-speed railway)

3. Identification of different numbers of carriages: As shown in Fig. 5(c), the number of obvious peaks (9 or 17) from the signal of the FBG strain sensors installed on the diaphragms of two box girders are used to determine the number of train carriages (8 or 16).

Based on this online identification method, the acceleration responses can be divided into nine parts corresponding to nine loading cases. The first eight loading cases only involve single trains running on the bridge, whereas the ninth loading case involves multiple trains running on the bridge. The first step of the online identification method is to distinguish the loading cases with a single train (Cases 1–8) and loading cases with multiple trains (Case 9). The loading cases with a single train (Cases 1–8) crossing the bridge refer to the acceleration responses featured by a single peak. Acceleration responses presenting multiple peaks belong to Case 9, with multiple trains crossing the bridge. Because of the complex characteristics of the multiple trains running on the bridge, this study only selects the responses of the first eight loading cases to analyze the correlations of speed acceleration. The eight loading cases with single trains running on the bridge are listed in Fig. 6.

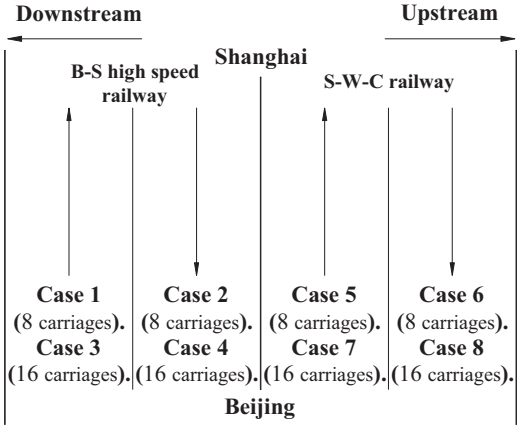

Fig. 6. Loading cases adopted for the Dashengguan Yangtze River Bridge

Early Warning of Abnormal Train-Induced Bridge Vibration

In the long-term service period of high-speed railway bridges, the serious overload of trains, deterioration of track irregularity on the main spans and approach spans, or damaged bridge components may lead to abnormal changes of train-induced vibration, especially the abnormal increase of acceleration responses. Therefore, it is very important to detect the abnormal changes of train-induced vibrations as early as possible, and it is meaningful to determine early warning thresholds of abnormal vibration for high-speed railway bridge maintenance. However, due to their random nature, the bridge acceleration responses have random fluctuations at different train speeds. Thus, it is necessary to determine the normal upper and lower thresholds of train-induced vibration responses from the viewpoint of probability. A two-stage method is developed to obtain the early warning thresholds of abnormal train-induced vibration by (1) extracting the median line of speed-acceleration correlations by wavelet packet decomposition and (2) calculating the early warning thresholds of acceleration fluctuation around the median line by interval estimation theory.

Median Line of Speed-Acceleration Correlation

After establishing the scatterplots of bridge acceleration amplitude and train speed, a median line of speed-acceleration correlation was constructed to analyze the trend of bridge acceleration amplitude varying with train speed.

First, sort a sequence of bridge acceleration amplitude data as

$$\boldsymbol{A}_{\mathrm{s}} = [A_{\mathrm{s}1}, A_{\mathrm{s}2}, \cdots, A_{\mathrm{s}i}, \cdots, A_{\mathrm{s}n}] \tag{1}$$

where n = length of $\boldsymbol{A}_{\mathrm{s}}$; and $A_{\mathrm{s}i}$ = ith element of $\boldsymbol{A}_{\mathrm{s}}$, where the subscript s$i$ is the corresponding train speed of $A_{\mathrm{s}i}$; and s1 < si < sn.

Then, the sequence of bridge acceleration amplitude $\boldsymbol{A}_{\mathrm{s}}$ was decomposed by a wavelet packet. The wavelet packet can decompose the speed-acceleration data to different scales (in appropriate scale), and the first decomposed sequence (in the lowest frequency band) of the last layer was extracted, which represents the trend of bridge acceleration amplitude varying with train speed. After multiple trials and reasonable selection of decomposition parameters, the median line of speed-acceleration correlation that best reflects the trend of bridge acceleration amplitude varying with train speed can

then be obtained. The principle of wavelet packet decomposition for a signal is as follows.

Based on two quadruple mirror filters $h_0(k)$ and $h_1(k)$, one discrete signal $x(d)$ can be decomposed scale by scale into different frequency bands (Figlus et al. 2014)

$$x_{0,0}(d) = x(d) \tag{2}$$

$$x_{j+1,2l}(d) = \sum_{i\in Z} h_1(i)x_{j,l}(2^j i - d) \tag{3}$$

$$x_{j+1,2l+1}(d) = \sum_{i\in Z} h_0(i)x_{j+1,l}(2^j i - d) \tag{4}$$

where $x_{j+1,2l}(d)$ and $x_{j+1,2l+1}(d)$ denote the dth values of the signal in the $2l$th and $(2l+1)$th frequency bands of the $(j+1)$th scale, respectively. The signal values in the $(j+1)$th scale can be obtained by the jth scale; thus, signal values in all scales can be obtained through sequential analogy. The $2l$th and $(2l+1)$th frequency bands are $\left[(2l-1)f_s/2^{j+1}, 2lf_s/2^{j+1}\right]$ and $\left[2lf_s/2^{j+1}, (2l+1)f_s/2^{j+1}\right]$, respectively, where f_s is the sampling frequency. Furthermore, Fig. 7 shows the wavelet packet tree of the signal $x(d)$, where $x(d) = \boldsymbol{A}_s$; and its decomposed sequence in the mth frequency bands of the jth scale = $\boldsymbol{A}_{sj,m}$.

After the N-scale wavelet packet decomposition of bridge acceleration amplitude $\boldsymbol{A}_s$, the 0th decomposed sequence of the Nth layer is extracted by the N-scale wavelet packet decomposition as the trial value

$$\boldsymbol{A}_s^w = \left[A_{s1}^w, A_{s2}^w, \cdots, A_{si}^w, \cdots, A_{sn}^w\right] \tag{5}$$

Different trials have a different parameter N, and the mean of bridge acceleration amplitude of several subsequences with certain length can be used to determine the optimal value of the trial results. The processes are as follows.

First divide $\boldsymbol{A}_s$ into M subsequences as

$$\boldsymbol{A}_s = [\boldsymbol{A}_{s1}, \boldsymbol{A}_{s2}, \cdots, \boldsymbol{A}_{sk}, \cdots, \boldsymbol{A}_{sM}] \tag{6}$$

Then, the mean of bridge acceleration amplitudes of every subsequence $\bar{\boldsymbol{A}}_{sk}$ and the mean of the corresponding speeds $\bar{s}_k$ can be calculated. The mean of the acceleration amplitudes at the speed range of $[\bar{s}_k - 0.5, \bar{s}_k + 0.5]$ can also be calculated from the trial results $\boldsymbol{A}_s^w\{N\ 0\}$ and is defined as $\bar{\boldsymbol{A}}_{sk}^w$.

The mean square error (MSE) between $\bar{\boldsymbol{A}}_{sk}$ and $\bar{\boldsymbol{A}}_{sk}^w$ at the same speed $\bar{s}_k$ can be calculated as

$$\text{MSE} = \sqrt{\frac{\sum_{k=1}^{M}\left(\bar{\boldsymbol{A}}_{sk} - \bar{\boldsymbol{A}}_{sk}^{w}\right)^2}{M}} \tag{7}$$

The values of the parameter N with the minimum value of the MSE can be used to gain the median line of the speed-acceleration correlation

$$\boldsymbol{A}_s^m = \boldsymbol{A}_s^{ow} = \left[A_{s1}^{ow}, A_{s2}^{ow}, \cdots, A_{si}^{ow}, \cdots, A_{sn}^{ow}\right] \tag{8}$$

Determination of Warning Thresholds of Abnormal Train-Induced Vibration

Once the median line of the speed-acceleration correlation is obtained, the fluctuation of bridge acceleration amplitudes around the median line can be calculated. The fluctuation of bridge acceleration amplitudes comes mainly from the random passenger capacity of the train and track irregularity (track irregularity refers to the deviation of the actual geometrical line from the ideal line of the tracks, which will induce acceleration fluctuations due to dynamic interaction of the train wheel and the track). Effective estimation of the fluctuation of bridge acceleration amplitudes can help determine the warning thresholds of train-induced vibration. The fluctuation of bridge acceleration amplitudes can be expressed as

$$\boldsymbol{F}_A = \boldsymbol{A}_s - \boldsymbol{A}_s^m \tag{9}$$

Denoting the mean of $\boldsymbol{F}_A$ as μ and the standard deviation of $\boldsymbol{F}_A$ as σ, according to the probability estimation of bridge acceleration fluctuation and the median line value, the upper and lower limits of the warning threshold of train-induced vibration can be expressed as

$$\begin{aligned} I_{ai} &= A_{si}^m - (\mu + r\sigma) \\ I_{bi} &= A_{si}^m + (\mu + r\sigma) \end{aligned} \tag{10}$$

where I_{ai} and I_{bi} = lower and upper limits of the warning threshold of A_{si}, respectively; A_{si}^m = corresponding median line value of A_{si}; and r is a correction coefficient that describes the dispersion degree of the fluctuation and is based on experience.

Because the bridge vibration responses vary with train speed, the estimation of μ and σ should be an interval corresponding to different train speeds. However, the point estimation method uses the same estimation parameters to describe the entire interval of

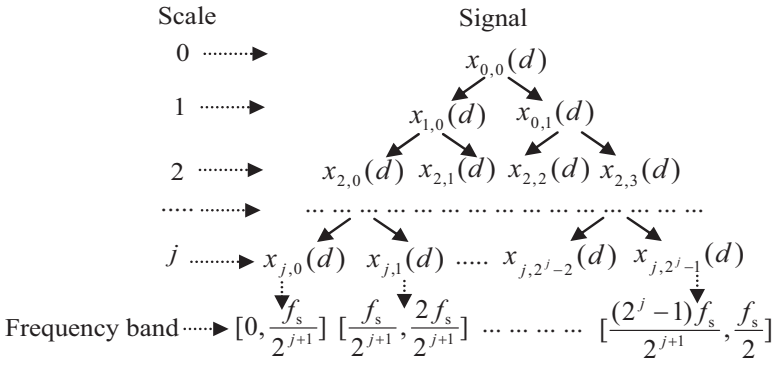

Fig. 7. Wavelet packet tree of the signal $x(d)$

samples, which will result in serious estimation errors for some speed intervals and cause a large number of sample points outside of the interval at a particular confidence level. This is known as the marginal effect. The marginal effect will lead to many speed-acceleration points overflowing the upper and lower limits when using the point estimation method. In the case of interval estimation (Chen and Cheng 2017), different probability parameters are used for different sample intervals, and this refinement probability estimate is needed for a better probabilistic description of bridge acceleration fluctuation.

Based on the interval estimation theory, the upper and lower limits of the fluctuation of bridge acceleration amplitudes can be obtained. Dividing $\boldsymbol{F}_{\mathrm{A}}$ into m subsequences

$$\boldsymbol{F}_{\mathrm{A}} = [\boldsymbol{F}_{\mathrm{As1}}, \boldsymbol{F}_{\mathrm{As2}}, \cdots, \boldsymbol{F}_{\mathrm{As}j}, \cdots, \boldsymbol{F}_{\mathrm{As}m}] \tag{11}$$

where m = number of subsequences and the m should be set according to the density of the speed-acceleration data; and $\boldsymbol{F}_{\mathrm{As}i}$ = jth subsequence. In the following analysis it is assumed that every subsequence obeys a normal distribution, the mean of the jth subsequence is μ_j, and the standard deviation of the jth subsequence is σ_j. The estimated interval of μ_j and σ_j is $[\mu_{ja}, \mu_{jb}]$ and $[\sigma_{ja}, \sigma_{jb}]$ in the $(1-\alpha)\times 100\%$ confidence level.

Assuming that σ_j is unknown, then $[\mu_{ja}, \mu_{jb}]$ satisfies the following relationship:

$$\mu_{ja} = \bar{X}_j - \frac{S_j}{n/m} t_{\alpha/2}(n/m-1) \tag{12}$$

$$\mu_{jb} = \bar{X}_j + \frac{S_j}{n/m} t_{\alpha/2}(n/m-1) \tag{13}$$

where $\bar{X}_j$ = mean of the jth subsequence; S_j = standard deviation the jth subsequence; and $t_{\alpha/2}(n/m-1)$ = value of the quantile point for $n/m-1$ samples on the Student distribution.

Assuming that μ_j is unknown, then $[\sigma_{ja}, \sigma_{jb}]$ satisfies the following:

$$\sigma_{ja} = \sqrt{n/m-1}S_j / \sqrt{\chi^2_{\alpha/2}(n/m-1)} \tag{14}$$

$$\sigma_{jb} = \sqrt{n/m-1}S_j / \sqrt{\chi^2_{1-\alpha/2}(n/m-1)} \tag{15}$$

where S_j = standard deviation the jth subsequence; and $\chi_{\alpha/2}(n/m-1)$ and $\chi_{1-\alpha/2}(n/m-1)$ = values of quantile point $\alpha/2$ and quantile point $1-\alpha/2$ for $n/m-1$ samples on the Chi-square distribution.

After obtaining the estimated intervals of μ_j and σ_j ($[\mu_{ja}, \mu_{jb}]$ and $[\sigma_{ja}, \sigma_{jb}]$) of each subsequence, the fluctuation interval can be defined as

$$\begin{aligned} F_{ja} &= \mu_{ja} - r\sigma_{ja} \\ F_{jb} &= \mu_{jb} + r\sigma_{jb} \end{aligned} \tag{16}$$

where F_{ja} and F_{jb} = lower and upper limits of the fluctuation interval of the jth subsequence; and r is a correction coefficient based on experience, which describes the dispersion degree of the fluctuation.

The upper and lower thresholds of the warning thresholds for bridge acceleration on each subsequence can be calculated by the superposition of the fluctuation interval and median line

$$\begin{aligned} I_{wja} &= \bar{\boldsymbol{A}}^{\mathrm{m}}_{sj} + F_{ja} \\ I_{wjb} &= \bar{\boldsymbol{A}}^{\mathrm{m}}_{sj} + F_{jb} \end{aligned} \tag{17}$$

where $\bar{\boldsymbol{A}}^{\mathrm{m}}_{sj}$ = mean of median line value of speed-acceleration correlation of the jth subsequence. Then, the upper and lower thresholds of the warning thresholds for bridge acceleration amplitude can be expressed as

$$\begin{aligned} \boldsymbol{I}_{\mathrm{wa}} &= [I_{\mathrm{w1a}}, I_{\mathrm{w2a}}, \cdots, I_{\mathrm{w}ja}, \cdots, I_{\mathrm{w}ma}] \\ \boldsymbol{I}_{\mathrm{wb}} &= [I_{\mathrm{w1b}}, I_{\mathrm{w2b}}, \cdots, I_{\mathrm{w}jb}, \cdots, I_{\mathrm{w}mb}] \end{aligned} \tag{18}$$

Early Warning of Train Running Stability

The crossing high-speed train will excite the vertical, transverse, and longitudinal vibrations of the bridge structure, and the transverse vibration of the bridge will greatly affect the running stability of the train or even cause the derailment of the train. The results of the derailment test by the Technical Committee on Railways and Rolling Stock of Japan indicated that the train can be easily derailed when the transverse acceleration (TA) of the bridge reaches 0.1–0.2 times gravitational acceleration (JISC 2004). Therefore, the early warning of train running stability due to excessive transverse vibration is an important consideration in high-speed railway engineering.

Because the train-induced transverse vibration has a large effect on the running stability of high-speed trains, the early warning thresholds of train running stability should be determined. The European Committee for Standardization (CEN 2000), the Japanese Industrial Standards Committee (JISC 2004), and the National Railway Administration of the People's Republic of China (2016) used the wheel unloading rate (WUR), derailment coefficient (DC), transverse force (TF) between the wheel and the rail, and TA of the train to guide the design of high-speed railway bridges. The WUR is the ratio of the reduction of wheel vertical load caused by vibration to the static axle weight, and the DC is the ratio of TF to the vertical force between the wheel and the rail. The three codes give the same safe limits of train running parameters (Table 1) and suggest that these train running parameters should not go beyond the limits. The static axle weight of the electric multiple units (EMUs), which runs on the Dashengguan Yangtze River Bridge, is 166.6 kN (Chai et al. 2014; Zhao et al. 2017). Based on the calculation results of the train-bridge coupled model of the Dashengguan Yangtze River Bridge (Wei 2012), the WUR, DC, wheel–rail TF, and TA of the train are linearly related to the TA amplitude of the bridge. Table 1 shows the safe limits and the linear fitting functions with bridge TA [using the results by Wei (2012)].

Thus, the ratio of early warning thresholds to the safe limits in design code for train running parameters can be used to describe the safety level of the train–bridge system in this method

$$\mathrm{Ratio} = \frac{Trp_{\mathrm{ew}}}{Trp_{\mathrm{limit}}} \tag{19}$$

where Trp_{ew} and Trp_{limit} = monitoring value and safe limit value for train running parameters, respectively. If the ratio of one running parameter is near 100%, it indicates that the train is at risk of derailing and that the running stability of trains should be addressed.

Table 1. Safe Limit in Code and Linear Fitting Function of Train Running Parameters

Train running parameter	Safe limit	Linear fitting with bridge TA (mm/s^2)
WUR	0.6	WUR = $0.006639a + 0.1117$
DC	0.8	DC = $0.009605a + 0.0488$
Wheel–rail TF	10 + (static axle weight)/3 (kN)	TF = $0.4757a + 9.27$
TA of train	0.1 × (gravitational acceleration) (mm/s^2)	TA = $1.056a + 49.86$

Note: a denotes the TA amplitude of the bridge.

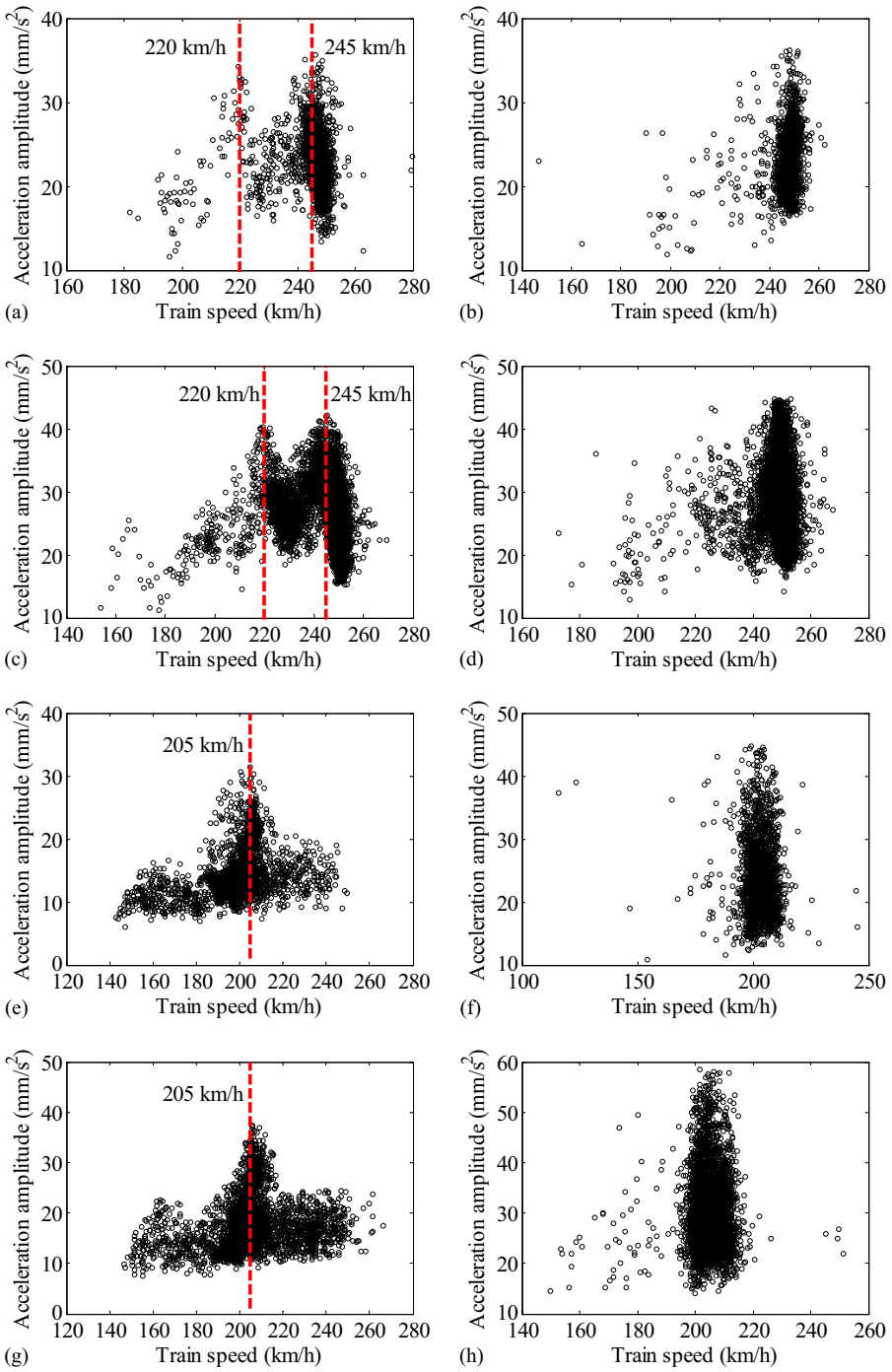

Fig. 8. Correlation scatterplots of TA and train speed: (a) Case 1; (b) Case 2; (c) Case 3; (d) Case 4; (e) Case 5; (f) Case 6; (g) Case 7; (h) Case 8

Results

Speed-Acceleration Correlations in Different Loading Cases

After distinguishing the bridge responses by the online identification of loading cases, the correlation scatterplots of TA and train speed in Cases 1–8 and correlation scatterplots of vertical acceleration and train speed in Cases 1, 3, 5, and 7 in Section 2 are shown in Figs. 8 and 9.

As shown in Figs. 8 and 9, the speed zone in Cases 2, 4, 6, and 8 is small and the data of train speeds are mostly based around the two speeds of 250 and 205 km/h. Therefore, it is difficult to investigate the correlations between bridge acceleration and train speed in Cases 2, 4, 6, and 8. Thus, the following correlation analysis between bridge acceleration and train speed will focus on Cases 1, 3, 5, and 7, in which it is found that the transverse and vertical acceleration amplitudes of the bridge increase at some specific train speeds, which are referred to as the peak speeds of the acceleration amplitude hereafter. The correlation scatterplots of bridge acceleration and train speed in Cases 1 and 3 show two peak speeds of bridge acceleration amplitude, whereas the correlation scatterplots of bridge acceleration and train speed in Cases 5 and 7 show only one peak speed of bridge acceleration amplitude. This phenomenon may be due to the different transverse loading positions between Cases 1 and 3 and Cases 5 and 7. For a four-lane wide bridge, such as the Dashengguan Yangtze River Bridge, different transverse loading positions of the train will excite different transverse or torsional mode shapes of the bridge, changing the train-induced vibrations and corresponding correlation scatterplots of bridge acceleration and train speed. This phenomenon is very complicated and should be investigated in future research. Furthermore, the speed-acceleration correlations in Cases 1 and 3 show similar trends, and the acceleration amplitude in Case 3 (with 16 carriages) is larger than the acceleration amplitude in Case 1 (with 8 carriages). Cases 5 and 7 have similar characteristics. Thus, the following early warning of train-induced vibration will focus on Cases 3 and 7 with 16 carriages.

Early Warning of Abnormal Train-Induced Vibration

As shown in Figs. 8 and 9, the scatterplots of the bridge acceleration and train speed show obvious correlations. A two-stage method is developed to obtain the early warning thresholds of abnormal train-induced vibration. As shown in Fig. 10(a), the four trials use the 0th sequence of the Nth layer with Nth scale wavelet packet decomposition, where $N = 6$, 7, 8, and 9. The corresponding MSEs of the four trials are 0.6926, 0.5737, 0.4105, and 2.3121 mm/s^2, respectively. The wavelet basis of symlets (Goswami and Chan 2011) is used for these trials of wavelet packet decomposition. Fig. 10(b) shows the optimal median line using wavelet packet decomposition ($N = 8$ and $I = 0$).

Then, based on the probability estimation theory, the lower and upper limits of the typical correlation scatterplots of bridge acceleration and train speed for Case 3 in Section 2 are shown in Fig. 11. As shown in Fig. 11, the probability estimation can only give two lines for the lower and upper limits with similar fashion, and the probability estimation shows a significant marginal effect for the data at a train-speed range of 2 4 5–255 km/h. Therefore, the warning thresholds obtained using the probability estimation theory will lead to a false alarm.

By using the interval estimation theory, the upper and lower limits of the typical correlation scatterplots of bridge acceleration and train speed can be obtained with a confidence level of 95% (with $\alpha = 0.05$). Fig. 12 shows the lower and upper limits of the fluctuation interval for the typical correlation scatterplots of bridge acceleration and train speed for Case 3 in Section 2. As shown in Fig. 12, the upper and lower limits obtained using interval estimation theory can be used to describe the random fluctuations of bridge accelerations around the median line regarding different train speeds. Figs. 13 and 14 show the typical early warning thresholds for train-induced vibration in Section 2. When the speed-acceleration data exceed the warning thresholds, it indicates abnormal changes of train-induced

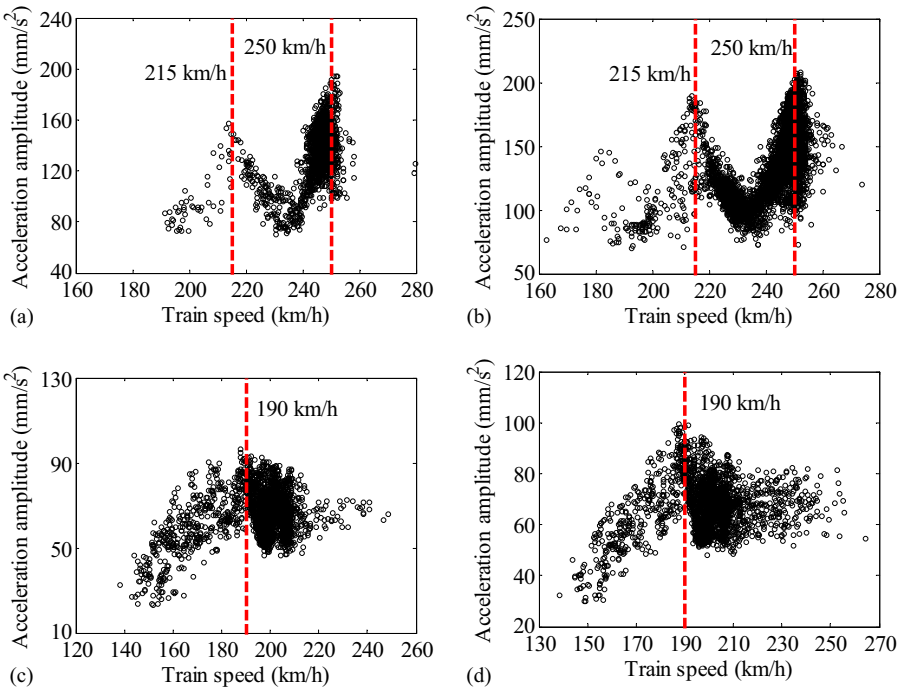

Fig. 9. Correlation scatterplots of vertical acceleration and train speed: (a) Case 1; (b) Case 3; (c) Case 5; (d) Case 7

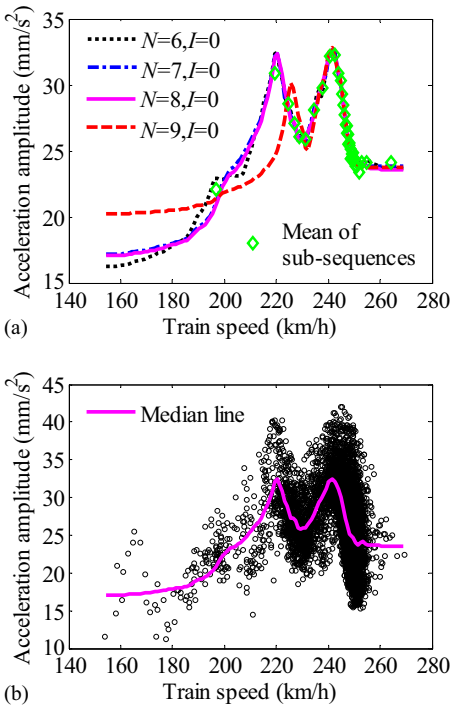

Fig. 10. Determination of median line of speed-acceleration correlations for transverse vibration in Case 3 in Section 2: (a) four trials using wavelet packet decomposition; (b) optimal value for median line

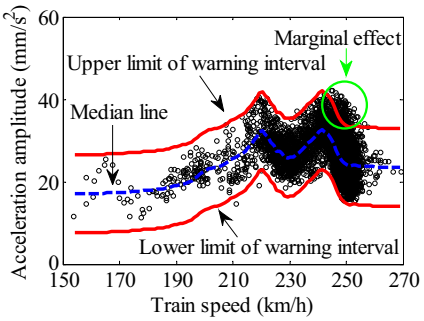

Fig. 11. Early warning threshold in Case 3 in Section 2 using the probability estimation

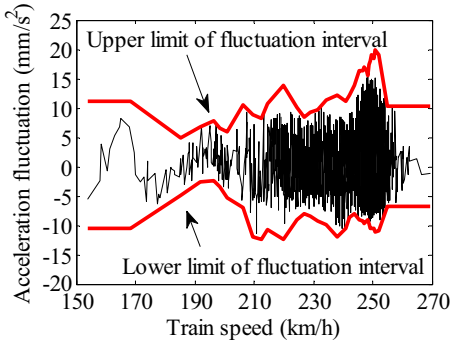

Fig. 12. Upper and lower limits of fluctuation interval in Case 3 in Section 2 using interval estimation (95% confidence)

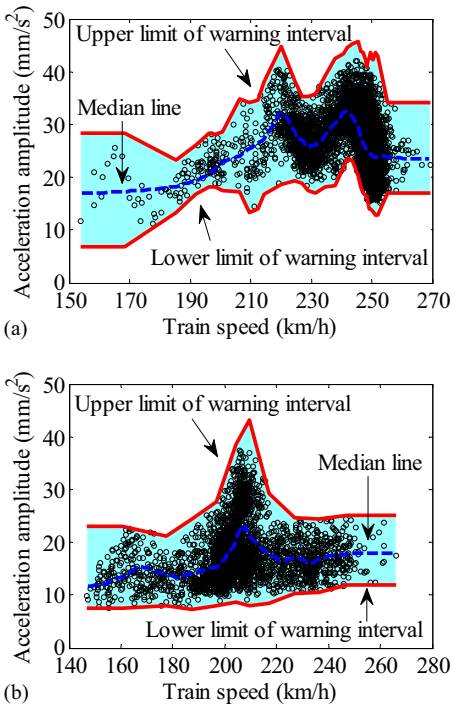

Fig. 13. Typical early warning thresholds of train-induced transverse vibration in Section 2: (a) Case 3; (b) Case 7

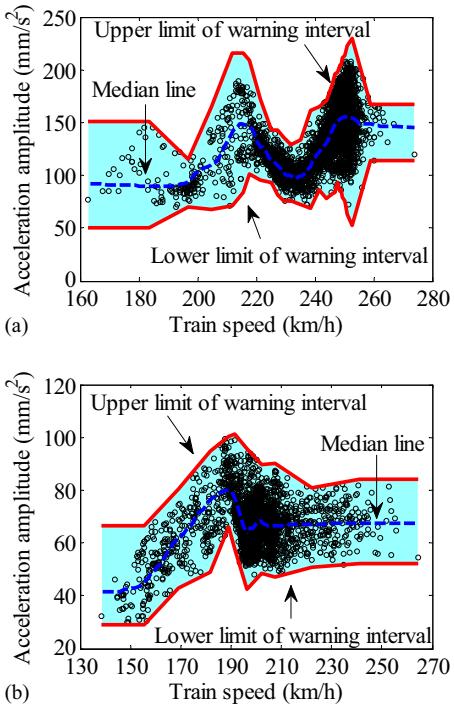

Fig. 14. Typical early warning thresholds of train-induced vertical vibration in Section 2: (a) Case 3; (b) Case 7

vibration, which is likely due to the serious overload of trains, deterioration of track irregularity on the main spans and approach spans, or damaged bridge components. Thus, more attention should be paid to the bridge and maintenance may be needed.

Early Warning of Train Running Stability

By using the warning thresholds of TA amplitudes obtained using the interval estimation theory in the previous section, the warning thresholds of train running parameters can be calculated by the functions in Table 1. Figs. 15 and 16 and Table 2 show the early warning thresholds of train running parameters due to train-induced transverse vibrations in Section 2 in Cases 3 and 7.

As shown in Figs. 15 and 16 and Table 2, although the train running parameters of the Dashengguan Yangtze River Bridge are all within safe limits, the WUR has reached 70% of the corresponding limit, and the DC approaches 60% of the limit at the maximum acceleration amplitude. Therefore, the effects of train-induced

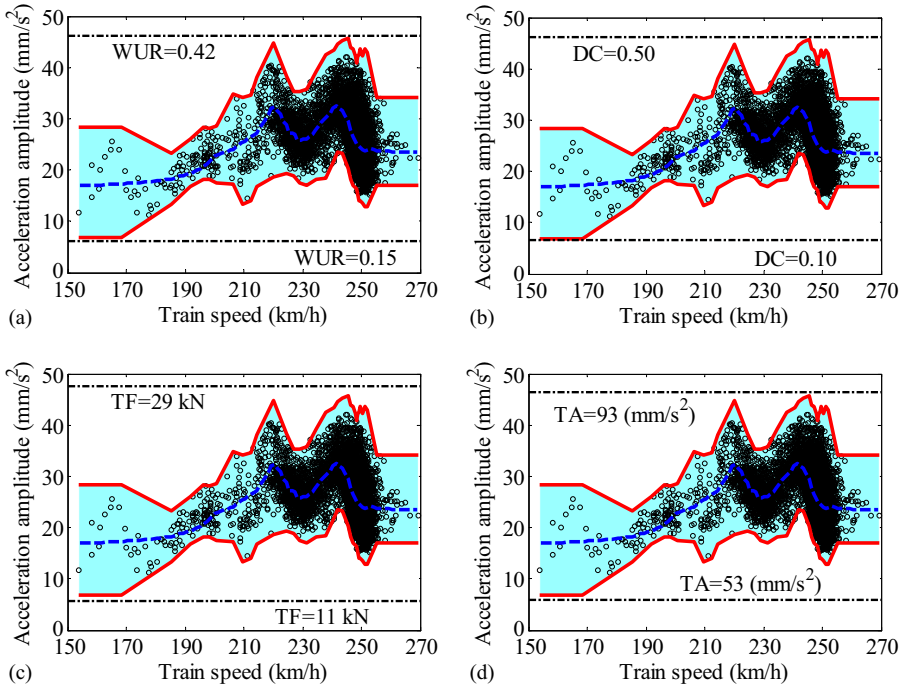

Fig. 15. Early warning thresholds of train running parameters due to train-induced transverse vibration in Case 3 in Section 2: (a) WUR; (b) DC; (c) wheel–rail TF; (d) TA of train

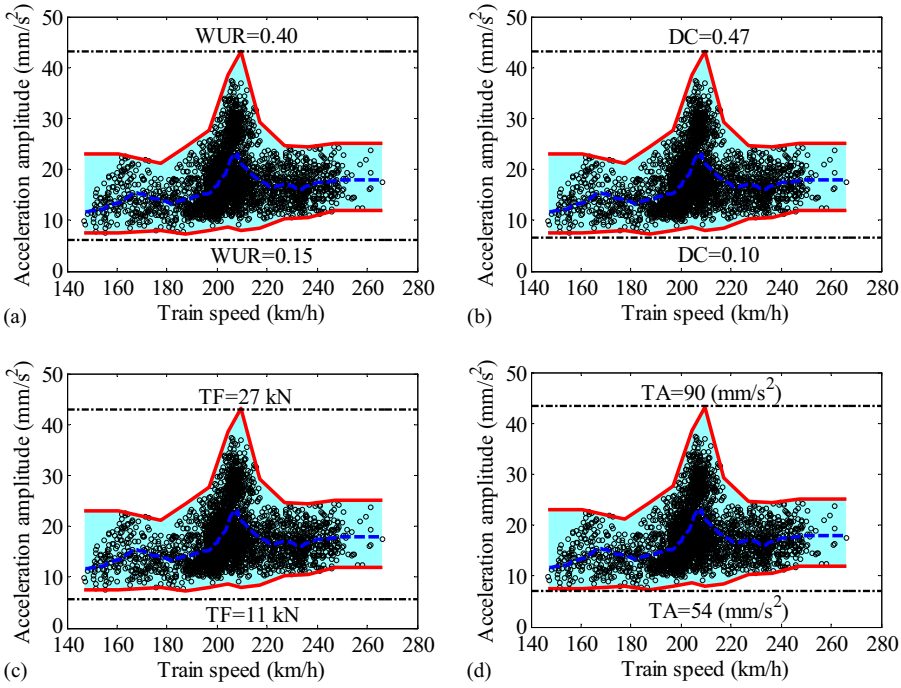

Fig. 16. Early warning thresholds of train running parameters due to train-induced transverse vibration in Case 7 in Section 2: (a) WUR; (b) DC; (c) wheel–rail TF; (d) TA of train

Table 2. Safe Limit, Upper and Lower Thresholds in Cases 3 and 7, and Percentage of Upper Early Warning Threshold to Safe Limit of Train Running Parameters

Train running parameter	Safe limit	Upper/lower thresholds calculated by bridge acceleration (Case 3, Case 7)	Percentage of upper early warning threshold to safe limit (Case 3, Case 7)
WUR	0.6	0.42/0.15, 0.40/0.15	70, 66.7
DC	0.8	0.50/0.10, 0.47/0.10	62.5, 58.75
Wheel–rail TF	65.5 (kN)	29/11, 27/11	44.3, 41.2
TA of train	980 (mm/s^2)	93/53, 90/54	9.5, 9.2

transverse vibration on the train running stability are worthy of attention. If the average train speed reaches 300 km/h or above in the future, it is necessary to monitor the real-time train running stability when high-speed trains cross the bridge.

Conclusion

1. The bridge acceleration responses under the action of high-speed trains are obtained based on the SHM system of the Dashengguan Yangtze River Bridge. An online identification method of loading cases is developed using the signal of multiple FBG strain sensors and acceleration sensors of the bridge SHM system. The correlations between the train speed and the bridge acceleration under different loading cases are obtained. The results reveal that for wide bridges with four lanes, such as the Dashengguan Yangtze River Bridge, different loading cases have different features of speed-acceleration correlations due to the different eccentric loads caused by different loading positions (outer lane and inner lane). Loading cases with 8 and 16 carriages in the same lane show similar trends of speed-acceleration correlations; however, the acceleration amplitudes under the loading cases with 16 carriages are larger than those under the loading cases with 8 carriages.
2. A two-stage method for early warning of abnormal train-induced vibration in each loading case is developed. First, the median line of speed-acceleration correlations is extracted by wavelet packet decomposition. Then, early warning thresholds for abnormal vibrations are determined by the interval estimation theory. The results show that the traditional probability estimation (point estimation) will induce a significant marginal effect, and the warning thresholds based on the probability estimation theory will lead to a false alarm. The warning thresholds based on interval estimation theory can be used to describe the random fluctuation of bridge accelerations in different train speed ranges and be used for the early warning of abnormal train-induced vibration.
3. The early warning method for train running stability is proposed. The relationships between train running parameters and bridge TA are obtained using the numerical results of the train-bridge coupled model of the Dashengguan Yangtze River Bridge. Then, the early warning thresholds for train running parameters can be calculated. The results show that the train running parameters of the Dashengguan Yangtze River Bridge are all within safe limits. However, the WUR and DC have reached over 60% of the limits due to train-induced transverse vibration. Therefore, the effects of train-induced transverse vibration on the train running stability is worthy of attention.

Acknowledgments

The authors gratefully acknowledge the support of the National Basic Research Program of China (973 Program) (No. 2015CB060000), the National Natural Science Foundation of China (51438002 and 51578138), the Scientific Research Foundation of Graduate School of Southeast University (No. YBJJ1657), the Fundamental Research Funds for the Central Universities (No. 2242016K41066), the Innovation Plan Program for Ordinary University Graduates of Jiangsu Province (No. KYLX16_0251), and A Project Funded by the Priority Academic Program Development of Jiangsu Higher Education Institutions (PAPD). The author gratefully acknowledges the support of the China Railway Major Bridge Reconnaissance & Design Institute Co., Ltd. and China Railway Major Bridge (Nanjing) Bridge and Tunnel Inspect & Retrofit Co., Ltd. It is acknowledged that the first and second authors contributed equally to this paper and should be considered co-first authors.

References

CEN. (2000). "Railway applications—Structural requirements of railway vehicle bodies." *EN12663*, Technical Committee CEN/TC 256 Railway Applications, Brussels, Belgium.

Chai, W., Wang, Q. X., Sun, J. J., and Wu, W. H. (2014). "The strength analysis of the pressed interference influences on CRH3 EMU wheel." *Mech. Eng. Technol.*, 3, 107–117 (in Chinese).

Chen, J. Y., and Cheng, C. H. (2017). "Reliability of stress–strength model for exponentiated Pareto distributions." *J. Stat. Comput. Simul.*, 87(4), 791–805.

Deng, L., He, W., and Shao, Y. (2015). "Dynamic impact factors for shear and bending moment of simply-supported and continuous concrete girder bridges." *J. Bridge Eng.*, 10.1061/(ASCE)BE.1943-5592.0000744, 04015005.

Dinh, V. N., Kim, K. D., and Warnitchai, P. (2009). "Dynamic analysis of three-dimensional bridge–high-speed train interactions using a wheel–rail contact model." *Eng. Struct.*, 31(12), 3090–3106.

Feng, D., and Feng, M. (2015). "Model updating of railway bridge using in situ dynamic displacement measurement under trainloads." *J. Bridge Eng.*, 10.1061/(ASCE)BE.1943-5592.0000765, 04015019.

Figlus, T., Liscak, S., Wilk, A., and Lazarz, B. (2014). "Condition monitoring of engine timing system by using wavelet packet decomposition of an acoustic signal." *J. Mech. Sci. Technol.*, 28(5), 1663–1671.

Goswami, J. C., and Chan, A. K. (2011). *Fundamentals of wavelets: Theory, algorithms, and applications*, 2nd Ed., John Wiley & Sons, Hoboken, NJ.

He, X. H., Yu, Z. W., and Chen, Z. Q. (2008). "Finite element model updating of existing steel bridge based on structural health monitoring." *J. Cent. South Univ. Technol.*, 15(3), 399–403.

JISC (Japanese Industrial Standards Committee). (2004). "Test methods of static load for truck frames and truck bolsters of railway rolling stock." *JIS E4208-2004*, Technical Committee on Railways and Rolling Stock, Tokyo (in Japanese).

Ju, S. H., and Lin, H. T. (2003a). "Numerical investigation of a steel arch bridge and interaction with high-speed trains." *Eng. Struct.*, 25(2), 241–250.

Ju, S. H., and Lin, H. T. (2003b). "Resonance characteristics of high-speed trains passing simply supported bridges." *J. Sound Vib.*, 267(5), 1127–1141.

Ju, S. H., Lin, H. T., and Huang, J. Y. (2009). "Dominant frequencies of train-induced vibrations." *J. Sound Vib.*, 319(1–2), 247–259.

Lacarbonara, W., and Colone, V. (2007). "Dynamic response of arch bridges traversed by high-speed trains." *J. Sound Vib.*, 304(1–2), 72–90.

Li, J. Z., and Su, M. B. (1999). "The resonant vibration for a simply supported girder bridge under high-speed trains." *J. Sound. Vib.*, 224(5), 897–915.

Mao, L., and Lu, Y. (2013). "Critical speed and resonance criteria of railway bridge response to moving trains." *J. Bridge Eng.*, 10.1061/(ASCE)BE.1943-5592.0000336, 131–141.

Martinez-Rodrigo, M. D., Lavado, J., and Museros, P. (2010). "Dynamic performance of existing high-speed railway bridges under resonant conditions retrofitted with fluid viscous dampers." *Eng. Struct.*, 32(3), 808–828.

Mellat, P., Andersson, A., Pettersson, L., and Karoumi, R. (2014). "Dynamic behaviour of a short span soil–steel composite bridge for high-speed railways–Field measurements and FE-analysis." *Eng. Struct.*, 69(Jun), 49–61.

National Railway Administration of the People's Republic of China. (2016). "Code for design of high speed railway." *TB 10621-2014*, Academy of Railway Sciences, Beijing (in Chinese).

Wei, Z. L. (2012). "Research on health monitoring system and condition assessment of large-scale high-speed railway bridge structure." Ph.D. dissertation, School of Civil Engineering, Southwest Jiao Tong Univ., Chengdu, China.

Xia, H., and Zhang, N. (2005). "Dynamic analysis of railway bridge under high-speed trains." *Comput. Struct.*, 83(23–24), 1891–1901.

Xia, H., Zhang, N., and Guo, W. W. (2006). "Analysis of resonance mechanism and conditions of train–bridge system." *J. Sound Vib.*, 297(3–5), 810–822.

Zhao, H., Ding, Y., An, Y., and Li, A. (2017). "Transverse dynamic mechanical behavior of hangers in the rigid tied-arch bridge under train loads." *J. Perform. Constr. Facil.*, 10.1061/(ASCE)CF.1943-5509.0000932, 04016072.

Zou, Q., Deng, L., and Jiang, C. (2016). "Predicting the bounds of vehicle-induced bridge responses using the interval analysis method." *J. Bridge Eng.*, 10.1061/(ASCE)BE.1943-5592.0000911, 04016046.